The M 4 Core Project with *HST* – III. Search for variable stars in the primary field[*]

V. Nascimbeni,[1][†] L. R. Bedin,[1] D. C. Heggie,[2] M. van den Berg,[3,4]
M. Giersz,[5] G. Piotto,[1,6] K. Brogaard,[7,8] A. Bellini,[9] A. P. Milone,[10]
R. M. Rich,[11] D. Pooley,[12,13] J. Anderson,[9] L. Ubeda,[9] S. Ortolani,[1,6]
L. Malavolta,[1,6] A. Cunial[1,6] and A. Pietrinferni[14]

[1]*INAF – Osservatorio Astronomico di Padova, Vicolo dell'Osservatorio 5, I-35122 Padova, Italy*
[2]*School of Mathematics and Maxwell Institute for Mathematical Sciences, University of Edinburgh, Kings Buildings, Edinburgh EH9 3JZ, UK*
[3]*Anton Pannekoek Institute for Astronomy, University of Amsterdam, Science Park 904, 1098 XH Amsterdam, the Netherlands*
[4]*Harvard–Smithsonian Center for Astrophysics, 60 Garden Street, Cambridge, MA 02138, USA*
[5]*Nicolaus Copernicus Astronomical Center, Polish Academy of Sciences, ul. Bartycka 18, 00-716 Warsaw, Poland*
[6]*Dipartimento di Fisica e Astronomia 'Galileo Galilei', Università di Padova, Vicolo dell'Osservatorio 3, I-35122 Padova, Italy*
[7]*Stellar Astrophysics Centre, Department of Physics and Astronomy, Aarhus University, Ny Munkegade, 8000 Aarhus C, Denmark*
[8]*Department of Physics and Astronomy, University of Victoria, PO Box 3055, Victoria, BC V8W 3P6, Canada*
[9]*Space Telescope Science Institute, 3800 San Martin Drive, Baltimore, MD 21218, USA*
[10]*Research School of Astronomy and Astrophysics, The Australian National University, Cotter Road, Weston, ACT 2611, Australia*
[11]*Department of Physics and Astronomy, University of California, Los Angeles, CA 90095, USA*
[12]*Department of Physics, Sam Houston State University, Huntsville, TX 77341, USA*
[13]*Eureka Scientific, Inc., 2452 Delmer Street, Suite 100, Oakland, CA 94602, USA*
[14]*INAF – Osservatorio Astronomico di Teramo, Via M. Maggini, I-64100 Teramo, Italy*

ABSTRACT

We present the results of a photometric search for variable stars in the core of the Galactic globular cluster Messier 4 (M 4). The input data are a large and unprecedented set of deep *Hubble Space Telescope* WFC3 images (large programme GO-12911; 120 orbits allocated), primarily aimed at probing binaries with massive companions by detecting their astrometric wobbles. Though these data were not optimized to carry out a time-resolved photometric survey, their exquisite precision, spatial resolution and dynamic range enabled us to firmly detect 38 variable stars, of which 20 were previously unpublished. They include 19 cluster-member eclipsing binaries (confirming the large binary fraction of M 4), RR Lyrae and objects with known X-ray counterparts. We improved and revised the parameters of some among published variables.

Key words: techniques: photometric – binaries: general – stars: variables: general – globular clusters: individual: NGC 6121.

1 INTRODUCTION

Messier 4 (M 4), also known as NGC 6121 is the closest Galactic globular cluster (GC) at 1.86 kpc, having the second smallest apparent distance modulus after NGC 6397: $(m - M)_V = 12.68$ (Bedin et al. 2009). It is known to show no evidence for any central brightness cusp, despite being significantly older than its dynamical relaxation time (Trager, King & Djorgovski 1995). Further, the photometric binary fraction in the core of M 4 is among the highest measured for a GC, reaching 15 per cent in the core region (Milone et al. 2012, compare with 2 per cent for NGC 6397). The fine details of the role played by dynamical interactions between binary stars in the delay of cluster 'core collapse' are still debated, with different competing theories proposed to explain them (see Heggie & Hut 2003 for a review). As M 4 appears to be a perfect case to test those theories, we proposed a *Hubble Space Telescope* (*HST*) large programme entitled 'A search for binaries with massive companions in the core of the closest GC M 4' (GO-12911, PI: Bedin), which has been awarded 120 orbits and has already been

successfully completed. The main aim of our project is to probe that fraction of binary population which is undetectable by means of usual photometric techniques, viz. the fraction that is made up of binaries composed of a main-sequence (MS) star and a massive, faint evolved companion (e.g. black hole, white dwarf, neutron star). The employed technique is an astrometric search for wobbles due to the motion of the bright component around the system barycentre. In support of this programme, a set of 720 WFC3/UVIS (Wide Field Camera 3, Ultraviolet and VISual channel) images have been gathered over a baseline of about one year. The UVIS 162 arcsec × 162 arcsec field of view (FOV) covers the whole core of M 4 (whose radius is $r_c \simeq 70$ arcsec; Harris 1996) at every roll angle. Of course, such a massive data set can be exploited for a large number of tasks other than the primary one. We will refer the reader to Paper I (Bedin et al. 2013) for a detailed description of the programme and for a discussion about other possible collateral science.

M 4 is a cluster that has some desirable properties for photometric searches of variables among Population II stars, viz. both its proximity and relatively low-density core. For this reason, it has been intensively targeted since the beginning of the photographic and photoelectric era (Leavitt & Pickering 1904; Sawyer 1931; Greenstein 1939; de Sitter 1947) up to more recent works which employed CCD photometry, either ground based (Kaluzny, Thompson & Krzeminski 1997; Kaluzny et al. 2013a) or space based (Ferdman et al. 2004). Besides a large number of known RR Lyrae (53, according to the online data base[1] compiled by C. Clement), eclipsing binaries and other ordinary variables, M 4 also hosts other less-common objects of interest, including an exotic planetary system made of a pulsar, a white dwarf (WD) and a 2.5 M_{jup} planet (Sigurdsson et al. 2003) and many X-ray sources (Bassa et al. 2004) whose optical counterparts show both periodic or irregular photometric variability (Kaluzny et al. 2012).

In this study, we exploit the GO-12911 data set to extract 9410 light curves of every well-measured, point-like source in the M 4 core, spanning from the horizontal branch down to the lower MS. We aim at discovering new variable stars and at refining the parameters of some others that were previously published; this includes the firm identification of a few objects for which the physical nature and/or the cluster membership was classified as 'uncertain' in the past. We describe in Section 2, the criteria adopted to select the input list, the procedures to correct the light curves by means of differential local photometry, and the specific algorithms employed to perform the search for periodic and irregular variability and to sift the most significant candidates. Then, in Section 3, we present our list of 38 high-confidence variables, along with a discussion of some notable individual cases. The overall statistics of our set, and in particular about its completeness limits and biases, is eventually discussed in Section 4.

2 DATA ANALYSIS

The full GO-12911 data set was gathered during 120 *HST* orbits, arranged in 12 epochs made of 10 *HST* visits each, where each visit is one orbit. Each orbit is filled with five 392–396 s exposures in the blue filter *F*467*M* (except for 11 isolated frames for which the *F*467*M* exposure time was set to 366 s), and one additional 20 s exposure through a red *F*775*W* filter at the beginning of the orbit.

[1] http://www.astro.utoronto.ca/~cclement/cat/listngc.html (Clement et al. 2001, last update 2009).

The choice of such unorthodox filters was driven by the astrometric requirements of our project. The intermediate band *F*467*M* yields a more monochromatic-like point spread function (PSF), less prone to colour-dependent systematic errors. For the same reason, the Sloan *i′*-like *F*775*W* filter was preferred over the more commonly used *F*814*W* thanks to its better characterized astrometric solution. Its ~1000 Å cut on the red tail does not imply a significant flux loss, because there the total transmission is very low. The *F*467*M* filter also has the advantage of suppressing the contaminating light of PSF haloes from red giants.

The first visit occurred on 2012 Oct 9, followed by a 100 d gap and then by 11 other visits regularly spaced at an ~24 d cadence. In this work, we will focus on a homogeneous subset of 589 'deep' (392–396 s) *F*467*M* images, in order to take advantage of a denser sampling and smaller flux contamination from giants. Data reduction was carried out by modelling an effective PSF (ePSF; Anderson & King 2000) tailored on each frame. Details about the ePSF approaches can be found in Paper I and references therein. Proper motions were derived by matching our data with Advanced Camera for Surveys (ACS) astrometry by Sarajedini et al. (2007, GO-10775, PI: Sarajedini), over a baseline of about six years.

It is worth noting that the codes employed are able to extract acceptable photometry even on stars brighter than saturation by collecting the charge bled along the columns of the detector (Gilliland 2004; Anderson et al. 2008). This is possible thanks to the excellent capability of WFC3/UVIS to conserve the flux even after the pixel full-well is exceeded (Gilliland, Rajan & Deustua 2010). Each unsaturated star in each exposure was measured by adding up the flux within its central 5 × 5 pixels, then dividing by the fraction of the star's light that should have fallen within the aperture (based on the PSF model and the PSF-fitted position of the stars within its central pixel). The aperture for saturated stars started with this 5 × 5 aperture, but we also had to include all contiguous pixels that were either saturated or neighbouring saturated pixels. The total flux was then the flux of the star through the aperture divided by the fraction of the PSF determined to lie within the aperture. In this way, we were able to determine the photometry of the saturated and unsaturated stars in the same system. Fig. 1 shows that the absolute precision of the saturated stars is not as good as that for the unsaturated stars, since the local zero-point (LZP) and global zero-point (GZP) are constructed to correspond to the 5 × 5 pixel aperture, not the variable aperture for saturated stars. Nevertheless, the smoothness of our colour–magnitude diagram (CMD; Fig. 3) across the *F*467*M* saturation boundary at −13.75 indicates that there are no systematic differences between photometry for the saturated and unsaturated stars. The reliability of this approach is shown by the quality of the light curves for the 13 RR Lyrae stars (see Section 3.1 for details).

Our initial input list was constructed by requiring the detection for each given source in at least 100 out of 589 frames, in order to get light curves spanning a phase coverage large enough to extract a meaningful period analysis from them. This constraint left us with 9410 sources, all brighter than instrumental magnitude *F*467*M* ≃ −4, corresponding to about 40 detected photoelectrons. On the bright side, the most luminous stars reach *F*467*M* ≃ −17.5 (corresponding to *V* ≃ 12.5: Fig. 1, upper-left panel). This means that the dynamic range of our data set spans more than 13 mag, enabling us to measure stars which are usually saturated and neglected in most surveys.

Most sources among our detections are single, point-like sources belonging to M 4. A small fraction of the sample, however, is made of galaxies, extended objects, unresolved stellar blends and
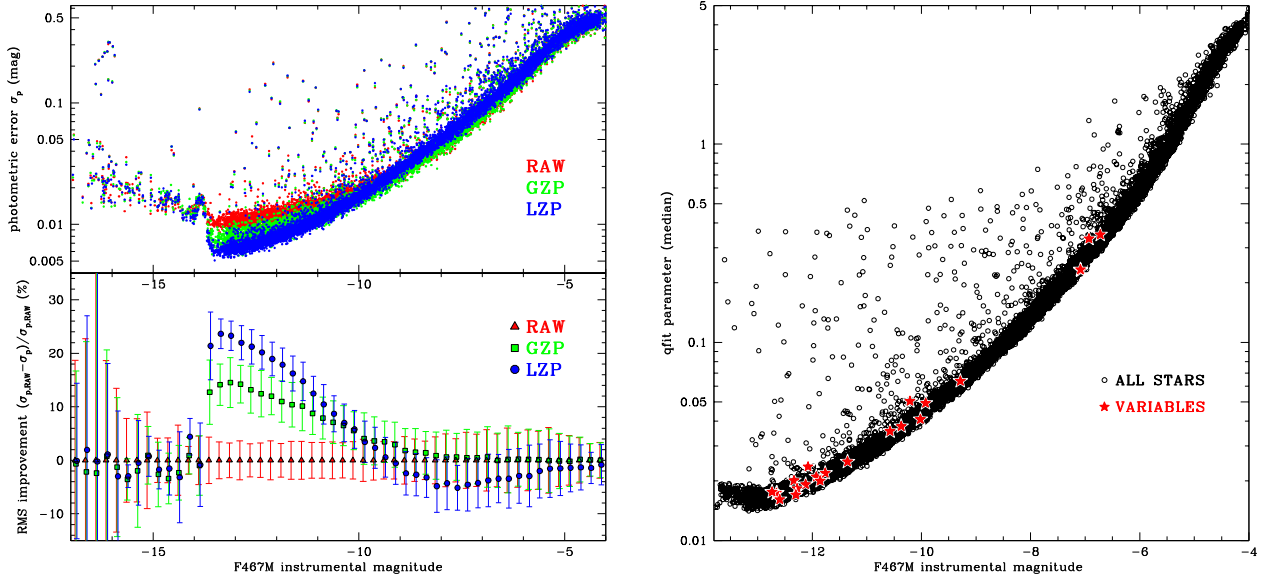
Figure 1. Left, upper panel: photometric error σ_p as a function of instrumental magnitude $F467M$, measured on all stars with three different correction algorithms: none ('RAW', red points), global zero-point ('GZP', green) and local zero-point ('LZP', blue). Saturation occurs at $F467M \simeq -13.75$. Left, lower panel: 'improvement' as a function of $F467M$, i.e. the per cent reduction of rms compared to raw light curves, averaged on 0.25 mag bins. Colours are coded as above. Right: median value of the fit quality parameter `qfit` as a function of $F467M$, all light curves (black circles). Variable stars found by our study (Table 1) are marked with red stars.

instrumental artefacts. These can be identified by looking at the `qfit` parameter, a diagnostic value that is related to the goodness of the ePSF fit (Anderson et al. 2008). As the mean $\langle$`qfit`$\rangle$ of a light curve is a monotonically increasing function of magnitude (Fig. 1, right-hand panel), a reliable way to identify badly measured outliers is to compare it with its median value evaluated over magnitude bins. We anticipate that, after the vetting procedure, all the variable stars discussed here are high-confidence point-like sources.

The observing strategy behind the GO-12911 programme was optimized for performing high-precision astrometry. In order to model and correct all the distortion terms of the astrometric solution, the images were gathered by setting a large-dither pattern of 50 points and changing the telescope roll angle within each astrometric epoch. Stars fall on completely different physical pixels on most frames. While this is a winning choice for the main goal of programme, it poses some issues when trying to extract accurate time-resolved photometry. Even when the PSFs are carefully modelled, this approach amplifies the effect of flat-field residual errors, intrapixel and pixel-to-pixel inhomogeneities, and other position-dependent effects. As a consequence, subtle second-order systematics are introduced in our photometry, as is evident by examining the raw light curves which share common trends whose shape and amplitude depend on the sky region analysed. A similar behaviour was also observed on data from the ACS/WFC in our previous work on NGC 6397 (Nascimbeni et al. 2012). Our approach to minimize such systematics is based on correcting differential light curves by subtracting a LZP, evaluated individually for each target star and each frame.

2.1 Global differential photometry

Before performing an LZP correction, an intermediate and straightforward step is applying a GZP correction. In what follows, we index the individual frames with variable i, the 9410 target stars with the variable k and the subset of sources chosen as comparison

stars with j. Individual data points from target/reference light curves will be then identified by $m_{i,k}$ and $m_{i,j}$, respectively. The notation $\langle x \rangle_y$ represents the averaging of x over the index y. Unless otherwise noted, averaging is done by evaluating the median and setting as the associated scatter $\sigma_{\langle x \rangle}$ the 68.27th percentile of the absolute residuals.

As a first step, we chose a common set of reference sources. These are required to be bright, non-saturated ($-13.75 < F467M < -10$), point-like and well-fitted (`qfit` within 2σ from the median `qfit` of all the stars having similar magnitude; this ensures that extended sources and blends are discarded). We also required that they are detected and measured on a minimum number of frames $N_{min} = 500$ over 589, as a reasonable compromise between completeness and FOV coverage. This left us with 1485 reference stars. For each of them, we computed the median raw magnitude $\langle m_{i,j} \rangle_i$ by iteratively clipping outliers at 2σ; then each reference raw light curve $m_{i,j}$ was normalized by subtracting $\langle m_{i,j} \rangle_i$ from it. A global 'trend' τ_i was calculated for each frame i by taking the 2σ clipped median of all available $m_{i,j} - \langle m_{i,j} \rangle_i$. The quantity τ_i is the GZP correction to be applied to each point $m_{i,k}$ belonging to target light curves

$$m'_{i,k} = m_{i,k} - \tau_i = m_{i,k} - \langle m_{i,j} - \langle m_{i,j} \rangle_i \rangle_j. \qquad (1)$$

The pre-normalization procedure enables us to estimate τ_i without biases, even if a small subset of reference stars is lacking from a given frame. On the other hand, median statistics, as opposed to arithmetic means and rms, proved to be robust enough against outliers.

If one plots the photometric scatter $\sigma_{\langle m \rangle}$ and $\sigma_{\langle m' \rangle}$ as a function of magnitude (Fig. 1, upper-left panel, red versus green points), it is clear that $\sigma_{\langle m' \rangle} < \sigma_{\langle m \rangle}$ especially on bright stars ($-13.5 < F467M < -10$). The average decrease in rms is up to 15 per cent at $F467M \simeq -13$ (Fig. 1, lower-left panel). GZP correction is therefore effective when compared to raw photometry. Still, upon visual inspection, spatial- and magnitude-dependent systematics are still present on

the bright side of our sample and require a more sophisticated correction.

2.2 Local differential photometry

In order to build a set of suitable reference light curves to evaluate an LZP correction, one needs to trim down the list of comparison stars by rejecting variables and badly behaved sources. First, we considered the distribution of GZP-corrected scatter $\sigma_{\langle m' \rangle}$ as a function of $\langle m'_{i,j} \rangle_i$, evaluating its median and scatter over magnitude bins; then each star more than 4σ off the median $\sigma_{\langle m' \rangle}$ was discarded from the reference set. The 'loose' 4σ threshold is justified by the need of not rejecting stars which could share common systematics with respect to other target stars; in that case their inclusion in the reference set would be the only way to correct such systematics.

For each pair of target star k and reference star j, we constructed a differential light curve by subtracting their raw magnitudes $m_{i,k}$ and $m_{i,j}$ on each frame i where both stars are detected. Then we considered the distribution of the absolute residuals around $\langle m_{i,k} - m_{i,j} \rangle_i$, and define the scatter σ_{jk} as the 68.27th percentile of such residuals. The quantity σ_{jk} is an empirical estimate of how much the reference star j is a 'good' reference for the target k. We can then assume the quantities $w_{jk} = 1/\sigma_{jk}^2$ as initial weights to compute a more accurate ZP correction for a given target k.

Since we want the correction to be *local*, we also multiply the weights by a factor D_{jk} which is dependent on the relative on-sky position $\varrho_{jk}^2 = (x_j - x_k)^2 + (y_j - y_k)^2$ between the reference star (x_j, y_j) and the target star (x_k, y_k). To avoid using a reference star too close to the target, which could therefore be blended or contaminated, D_{jk} is forced to zero within r_0. Outside r_0, we chose to parametrize D_{jk} as a unitary factor up to an inner radius r_{in}, and then as a smooth function which decreases exponentially from one to zero with a $r_{out} - r_{in}$ scale radius (i.e. the factor D_{jk} is $1/e$ at r_{out})

$$D_{jk} = \begin{cases} 0 & \text{if } \varrho_{jk} < r_0 \\ 1 & \text{if } r_0 \leq \varrho_{jk} \leq r_{in} \\ \exp\left[-\left(\frac{\varrho_{jk} - r_{in}}{r_{out} - r_{in}}\right)^2\right] & \text{if } \varrho_{jk} > r_{in}. \end{cases} \quad (2)$$

A similar weight factor M_{jk} is imposed on the magnitude difference $\phi_{jk} = |m_j - m_k|$, as we expect that systematics due to non-linearity and background estimation are magnitude dependent. The flux boundaries are f_{in} and f_{out}, respectively:

$$M_{jk} = \begin{cases} 1 & \text{if } \phi_{jk} \leq f_{in} \\ \exp\left[-\left(\frac{\phi_{jk} - f_{in}}{f_{out} - f_{in}}\right)^2\right] & \text{if } \phi_{jk} > f_{in}. \end{cases} \quad (3)$$

Summarizing, the final weights are given by multiplying the above factors:

$$W_{jk} = \left(1/\sigma_{jk}^2\right) D_{jk} M_{jk}. \quad (4)$$

The LZP correction τ_i' is evaluated as for the GZP correction (equation 1), but this time using the weighted mean of magnitudes of our set of reference stars instead of an unweighted median, where the weights are assigned as W_{jk}. A 3σ clip is applied on each image i to improve robustness.

Our approach gives larger weights to reference stars which (1) produce a smaller scatter on the target light curve; (2) are geometrically closer to the target as projected on the sky; (3) have a magnitude similar to that of the target. Of course, this approach could be easily generalized by introducing weights based on other external parameters, such as colour or background level, for instance.

The five input parameters $r_0, r_{in}, r_{out}, f_{in}, f_{out}$ have to be chosen empirically. After some iterations, we set $r_0 = 20$ pix, $r_{in} = 200$ pix, $r_{out} = 300$ pix, $f_{in} = 1.0$ mag, $f_{out} = 1.75$ mag. The improvement of the LZP correction over the GZP one is shown in the left-hand panel of Fig. 1. In the bright, non-saturated end of our sample ($F467M \simeq -13$) the rms is lowered by 10–25 per cent on average when compared to GZP-corrected and raw photometry, respectively. On the faintest targets, GZP performs slightly better than LZP because photon noise dominates and GZP is not forced to discard very bright stars as LZP does. For each target, we chose to apply an *optimal* correction which outputs the light curve having the lowest scatter among the raw one and the GZP- or LZP-corrected ones. From here on, all procedures are carried out on such optimal light curves.

2.3 Variable-searching procedures

A battery of software tools to detect both periodic and non-periodic photometric variability was applied to all 9410 corrected light curves. These tools included period-searching algorithms such as the classical Lomb & Scargle periodogram (LS; Lomb 1976; Scargle 1982) and its generalized version GLS (Zechmeister & Kürster 2009); the Analysis of Variance periodogram (AoV; Schwarzenberg-Czerny 1989); the Box-fitting Least-Squares periodogram (BLS; Kovács, Zucker & Mazeh 2002). The latter is the most sensitive to eclipse-like event, such as those expected from detached eclipsing binaries and planetary transits. A second class of diagnostics was exploited to search for more general types of variability: the alarm variability statistic as described by Tamuz, Mazeh & Zucker (2005), the overall scatter (based on robust median statistics as defined at the beginning of Section 2.1) as a function of magnitude, and the rms after each of the 12 astrometric epochs has been averaged on a single bin, to catch the effects of long-term variability.

We already mentioned that our data set is not optimized to search for periodic variability. One of the most limiting factors is the non-regular cadence, as each astrometric epoch is separated by 24 d. These temporal gaps introduce many spurious frequencies in the periodograms, making the recovery of the true (astrophysical) period problematic, especially for signals at $P < 24$ d where most of the variables are expected to be. We illustrate this by injecting noise-free sinusoids over the 589-images time baseline of our WFC3 data set, and then recovering the signal through a GLS periodogram on the synthetic light curve (Fig. 2). In both cases at $P_{inj} = 0.3$ and 4.0 d, we get a 'comb' of periodogram peaks instead of a sharp spike, as it would be expected in an optimal sampling regime. When random noise and systematic errors are accounted for, period recovering gets harder, and the 24 d alias induced by sampling becomes the most significant period. For this reason, we split our search over two period ranges: 0.1–20 and 20–200 d, analysing each set independently.

To visually supervise all the individual outputs of the analysis described above on more than 9000 targets would be too much time-consuming and prone to biases. Instead, we selected a short list of candidate variables by running the very same analysis on a set of synthetic light curves, sampled at the same epochs as the real data but after having randomly shuffled the magnitude values. In this way, noise and sampling cadence are preserved, while phase coherence is broken: the resulting 'synthetic' analysis represents the expected output when an intrinsic signal is not present. We focused on the distribution of diagnostics such as
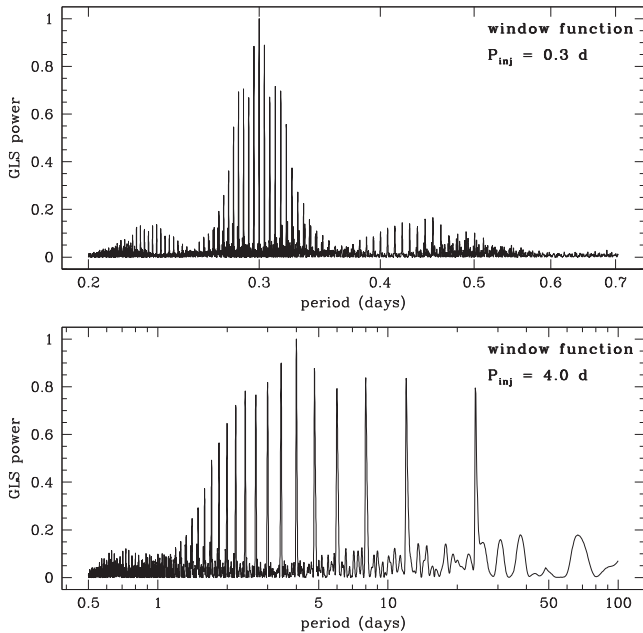
Figure 2. Noise-free window function computed over the temporal baseline of our data set; the injected periods are $P_{\mathrm{inj}} = 0.3$ d (upper panel) and $P_{\mathrm{inj}} = 4.0$ d (lower panel).

(i) the periodogram *power* for the LS, GLS and AoV algorithm (as defined in the original papers, i.e. P_X by Scargle 1982, $p(\omega)$ by Zechmeister & Kürster 2009, and Θ by Schwarzenberg-Czerny 1989, respectively);

(ii) the *SN* and *SDE* statistics (Kovács et al. 2002) and the signal-to-pink noise ratio (as defined by Pont, Zucker & Queloz 2006 and implemented by Hartman et al. 2008) for the BLS periodogram;

(iii) the alarm index $\mathcal{A}$ (Tamuz et al. 2005) and the visit-binned and unbinned rms as a function of magnitude, defined as above.

For each of the above diagnostics, the output distribution from the real data was compared with the results from the synthetic light curves, selecting all targets which fall at least 3σ outside the latter distribution. This gave us a list of 401 candidates which were individually inspected. Most of them turned out to be spurious, due to the target being blended, contaminated, or part of an extended source. Very often false positives came from sources with bad photometry on a single visit due to the star falling on a bad pixel or too close to the detector edges. The latter case was the most frequent cause of false positives detected at periods around the 12 or 24 d alias.

3 RESULTS

After the vetting process, only 38 variables survived. They are listed in Table 1; their light curves are plotted in Figs 4 and 5, and the corresponding data points are tabulated in Table 2. All of them appear to be isolated, point-like sources, following a visual inspection of the images. This is also confirmed by their `qfit` diagnostic, which is perfectly consistent with the median `qfit` of well-measured stars of similar magnitude (Fig. 1, right-hand plot; variables are marked with red stars). Their detected periods are clearly distinct from the typical periods due to aliasing or instrumental effects, such as the 96 min orbital period of *HST* or the 24 d separation between consecutive visits. For the reasons above, we can identify all those 38 stars as genuine astrophysical variables. In Table 1, we also report the Johnson *V*-band magnitude of each variable (obtained by

cross-matching our catalogue with that by Sarajedini et al. 2007) and we identify which stars are matched within a 2σ error ellipse with an X-ray source from the Bassa et al. (2004) catalogue. We stress out that the reported *V* magnitudes represent the average of the values obtained by Sarajedini et al., not an intensity-weighted average throughout the phase of our light curves.

The membership of our variables with respect to M 4 can be assessed with a very high level of confidence by inspecting the proper motion vector–point diagram (VPD), where stars belonging to the cluster and those in the general field appear extremely well separated (Fig. 3, upper-left plot). To our purposes, the VPD does not need to be calibrated in physical units (arcsec yr^{-1} proper motion); instead, we simply plot the displacement in pixels measured over the baseline between the WFC3 observations and the first astrometric ACS epoch ($\sim$6 yr). We found that nearly all variables are cluster members with the only exceptions being ID# 3407 and 3708. As expected, most variables found at magnitudes fainter than the cluster turnoff turned out to be eclipsing binaries, both of contact (cEB) and detached (dEB) subtypes. On most cases, this classification is also supported by their position on the CMD, which is shifted up to $\sim$0.75 mag upwards with respect to single, unblended MS stars (Fig. 3). A discussion of individual cases follows.

3.1 Notes on individual objects

Known RR Lyrae: ID# 1076, 1134, 1497, 2594, 4363, 6285, 6394, 6458, 6954, 8077, 8798. These are RR Lyr variables known since a long time (Greenstein 1939, re-identified by Shokin & Samus 1996), but whose periods are here determined with much more precision given the 1 yr temporal baseline. The discrimination between RRab (ID# 1076, 1134, 4363, 6394, 6458, 6954, 8077, 8798) and RRc (1497, 2594, 6285) subtypes is obvious. Our classification is confirmed by their position in the CMD (Fig. 3, right-hand panels), with RRab and RRc member being clearly separated by the RR Lyrae gap. The amplitudes of ID# 6285 and 8077 change significantly through the series, due possibly to the Blazhko effect (Kovács 2009).

New RR Lyrae: ID# 6858, 6955. These are two very close (1.6 arcsec) RR Lyr variables having similar magnitude ($V = 13.24$ versus 13.39). Such an unusual pair is mostly blended on ground-based images, so it is not surprising that it was classified by Greenstein (1939) as a single RR Lyr with a problematic light curve (C40) and a poorly constrained period. Other studies recognized it as a visual binary but failed at discovering the true nature of both sources (de Sitter 1947); therefore, C40 has been neglected in many follow-up works on RR Lyrae. We identified both stars as RRc subtypes with periods $P \simeq 0.39$ and 0.29 d, respectively.

Blue stragglers: ID# 1600 and 7820 are without any doubt cluster members based on their proper motions, and are located in the 'blue straggler' region of the CMD. ID# 1600 was already known as a short-period, near equal-mass contact eclipsing binary (Kaluzny et al. 1997). ID# 7820 also is a contact binary, reported here for the first time. Its periodic modulation at $P \simeq 0.66$ d is detected at high significance. Its primary and secondary minima, showing very unequal depths, suggest a much lower mass ratio than ID# 1600.

Known contact EBs: ID# 3401, 3407, 5430, 6807 are already listed in the Clement et al. (2001) catalogue. They are located close to the turnoff region, with very well-defined primary and secondary minima and periods spanning 0.26–0.30 d. Among these, ID# 3407 is the only field star, clearly separated from the cluster in the proper motion (PM) diagram; also it is an X-ray source catalogued as CX13 by Bassa et al. (2004).

Table 1. Variables found and their characteristics.

N	ID#	α (J2000)	δ (J2000)	F467M	V	M	Type	P (d)	X-ref	Notes
1	275	245.904 61	− 26.550 51	− 7.08	21.77	Y	cEB	0.183 163	–	MS
2	760	245.888 14	− 26.553 50	− 6.65	22.03	Y	dEB	0.378 524	–	BSEQ
3	1001	245.922 83	− 26.534 79	− 10.02	19.30	Y	EB?	0.629 85	–	BSEQ
4	1076	245.894 37	− 26.547 83	− 16.00	13.56	Y	RRab	0.623 998	C39	HB
5	1134	245.886 84	− 26.550 99	− 15.94	13.91	Y	RRab	0.577 852	C38	HB
6	1497	245.897 38	− 26.543 33	− 16.40	13.30	Y	RRc	0.309 436	C20	HB
7	1600	245.910 36	− 26.536 34	− 13.88	15.74	Y	cEB	0.308 446	C72=K53	BSS
8	2108	245.895 80	− 26.540 05	− 10.36	18.96	Y	dEB	6.853 342$^{‡?}$	–	BSEQ; CX28
9	2316	245.889 63	− 26.541 61	− 10.21	19.17	Y	EB	1.936 34	–	BSEQ; CX25
10	2594	245.905 45	− 26.532 28	− 16.32	13.05	Y	RRc	0.298 536	C23	HB
11	2992	245.896 16	− 26.534 45	− 11.76	17.64	Y	EB?	3.208 466	–	MS/BSEQ
12	3153	245.894 46	− 26.534 51	− 10.57	18.91	Y	EB	2.694 56	–	MS/BSEQ; CX21
13	3236	245.908 70	− 26.527 18	− 12.65	16.89	Y	EB?	3.207 522	–	BSEQ/TO; CX3
14	3401	245.903 29	− 26.528 91	− 12.66	16.79	Y	cEB	0.282 687	C67=K48	TO; CX15
15	3407	245.893 02	− 26.533 85	− 12.08	16.98	N	cEB	0.297 443	C68=K49	NM; CX13
16	3487	245.902 70	− 26.528 71	− 9.93	19.30	Y	EB	2.071 346	–	BSEQ
17	3575	245.915 44	− 26.522 22	− 9.29	19.85	Y	EB	3.896 14	–	BSEQ
18	3627	245.903 75	− 26.527 55	− 11.36	18.09	Y	EB	2.190 352	–	MS/BSEQ; CX20
19	3708	245.906 34	− 26.525 92	− 12.33	17.17	N	dEB	>6.476	–	NM; one eclipse
20	4363	245.899 60	− 26.526 04	− 15.97	13.70	Y	RRab	0.472 028	C21	HB
21	5286	245.898 08	− 26.522 31	− 6.92	21.87	Y	dEB	5.272 694‡	–	BSEQ
22	5430	245.880 48	− 26.530 14	− 12.13	17.53	Y	cEB	0.265 997	C69=K50	MS
23	5460	245.884 32	− 26.528 12	− 12.73	16.80	Y	dEB	8.111	K66	TO
24	6285	245.881 55	− 26.525 19	− 16.27	13.60	Y	RRc	0.247 351	C37	HB
25	6394	245.908 40	− 26.511 61	− 16.12	13.36	Y	RRab	0.546 796	C24	HB
26	6458	245.894 48	− 26.517 95	− 15.92	13.72	Y	RRab	0.478 81	C18	HB
27	6807	245.888 31	− 26.519 17	− 12.28	17.08	Y	cEB	0.303 677	C70=K51	BSEQ
28	6858	245.901 95	− 26.512 30	− 16.41	13.24	Y	RRc	0.385 321	C40†	HB
29	6873	245.893 21	− 26.516 36	− 11.93	17.56	Y	dEB	3.358 846‡	–	BSEQ
30	6954	245.914 15	− 26.505 92	− 16.18	13.07	Y	RRab	0.612 751	C25	HB
31	6955	245.901 69	− 26.511 90	− 16.23	13.39	Y	RRc	0.286 246	C40†	HB
32	7202	245.868 87	− 26.526 11	− 12.30	17.20	Y	dEB	5.925 962$^{‡?}$	–	BSEQ
33	7820	245.902 61	− 26.506 05	− 14.02	15.76	Y	cEB	0.660 748	–	BSS
34	7864	245.881 11	− 26.516 06	− 12.58	16.92	Y	UNK	–	C71=K52	Above BSEQ; CX8
35	8077	245.903 87	− 26.503 62	− 16.09	13.17	Y	RRab	0.603 037	C22	HB
36	8081	245.885 01	− 26.512 63	− 11.86	17.65	Y	UNK	0.971 994	–	BSEQ; CX11
37	8798	245.885 32	− 26.506 39	− 16.09	13.55	Y	RRab	0.542 544	C16	HB
38	9050	245.893 51	− 26.499 84	− 7.09	21.95	Y	cEB?	0.185 888	–	Under the MS

Notes. The columns give: a progressive number *N*, the ID code of the source according to our catalogue, the equatorial coordinates α and δ at epoch 2000.0, the instrumental magnitude in *F*467*M* and the standard Johnson *V* magnitude from Sarajedini et al. (2007), a membership flag derived from the VPD, the variability class assigned by our study, the most probable photometric period *P* (where detectable), the cross-references to the variable catalogues by Kaluzny et al. (2013a, letter K) and Clement et al. (2001, letter C), and some notes. Notes are codified as follows: MS = main-sequence star, BSEQ = binary sequence star (between fiducial MS and MS+0.75 mag), HB = horizontal branch, BSS = blue straggler star, CX = X-ray source from the catalogue by Bassa et al. (2004), TO = turn-off star, NM = not a cluster member. A few periods of dEBs, marked with a ‡, have been doubled with respect to the best-fitting periodogram solution, following astrophysical arguments (see Section 3.1 for details); two cases are ambiguous, and marked with an additional question mark. The two variables marked by † in the X-ref field were once classified as a single, atypical RR Lyr (Clement et al. 2001 and references therein).

Detached EBs: ID# 760, 2108, 3708, 5286, 5460, 6873, 7202 are detached eclipsing binaries, all identified as cluster members by PMs with the only exception of ID# 3708. Among them only ID# 5460 was previously published (as K66 by Kaluzny et al. 2013a). All of them lie in the upper part of the binary MS, i.e. are systems with high mass ratios (*q* ≈ 1). For that reason, their phased light curves are expected to show two eclipses of similar depth between phases 0 and 1. But the period-search algorithms does not know this and therefore might find periods of half the true duration with light curves showing only one eclipse between phases 0 and 1. In some cases, such as for ID# 2108, we have no way of knowing the true period with the current data because of holes in the phased light curves where an eclipse might be happening. In other cases, such as for ID# 5286, the phase coverage seems sufficient to rule out the presence of a second eclipse at the period found, which suggests that the true period is twice as long. Based on such considerations, we give the most likely true periods in Table 1. ID# 2108 also is an X-ray source (CX 28; Bassa et al. 2004), but its light curve shows no

Table 2. Light curves of the variables found.

ID#	BJD(TDB)	*F*467*M*	$\Delta F467M$	*x*	*y*	qfit
1001	2456209.701194	− 10.0180	0.0168	2653.966	2571.443	0.037
1001	2456209.740334	− 10.0160	0.0168	2653.973	2571.472	0.046
1001	2456209.746422	− 10.0060	0.0168	2653.999	2571.477	0.032
1001	2456209.752509	− 10.0130	0.0168	2653.973	2571.466	0.039
1001	2456209.764684	− 9.9920	0.0168	2653.994	2571.487	0.031
1001	2456209.806845	− 10.0040	0.0168	2654.001	2571.439	0.033
1001	2456209.812933	− 10.0110	0.0168	2653.990	2571.455	0.037
1001	2456209.819020	− 10.0080	0.0168	2653.991	2571.449	0.039
1001	2456209.825108	− 10.0200	0.0168	2653.965	2571.461	0.037
1001	2456209.831195	− 10.0035	0.0168	2653.963	2571.475	0.048

Notes. This table is published in its entirety as a machine-readable table in the online version of this article and the Centre de Donees Strasbourg (CDS) at http://cdsarc.u-strasbg.fr/viz-bin/qcat?J/MNRAS/. A portion is shown here for guidance regarding its form and content. The columns give: the ID code of the source according to our catalogue (see Table 1), the mid-exposure time in the BJD–TDB time standard (Eastman, Siverd & Gaudi 2010), the instrumental magnitude in *F*467*M* and the associated photometric error, the *x* and *y* centroid position on the chip, and the qfit quality parameter.

sign of stellar activity or interaction. We set the period of ID# 3708 as a lower limit ($P > 6.47$ d) since only one eclipse is detectable in our series.

New contact and generic EBs: ID# 2316, 3153, 3487, 3575. The light curves of ID# 2316 and 3153 show an anomalous amount of scatter despite being isolated and well-measured (low qfit); this could be ascribed to starspot-induced variability by one or both components of the eclipsing binary. ID# 3487 is a much fainter EB in the lower MS, observed at low S/N but with recognizable minima and maxima.

Probable EBs: ID# 1001, 2992, 3236, 3627. ID# 1001 shows a sharp ∼0.1 mag eclipse overimposed on a pseudo-sinusoidal modulation. If the modulation is interpreted as caused by a 'hotspot' or persistent active region then the eclipse appears to be out of phase by about 0.25 (assuming circular orbits, and spin–orbit alignment). No secondary minimum is detected. Light curves of ID# 2992, 3236, 3627 share similar amplitudes (0.05–0.1 mag) and an excess of photometric scatter, but their position in the CMD makes a cEB/dEB classification plausible. ID# 3236 (=CX3) and 3627 (=CX20) are also matched to X-ray sources.

Unclassified/uncertain: ID# 275, 7864, 8081, 9050. The light curve of ID# 275 is clearly periodic with a 'double-wave' shape and minima of similar depths. Anyway, its period $P \simeq 0.18$ d is smaller than the usual ∼0.22 d cut-off found for MS+MS eclipsing binaries (Norton et al. 2011) and its position on the CMD is very close to the MS ridge, disproving the presence of companions with high *q*. On the other hand, ID# 275 could be a new member of the recently discovered class of ultra-short-period M dwarf binaries, first introduced by Nefs et al. (2012). ID# 7864 is a known variable and X-ray source (K52; CX8), and is much brighter than the upper binary sequence envelope, revealing itself as an interacting and/or higher multiplicity system. This is confirmed by its light curve, showing a strong $P \simeq 0.77$ d periodicity but also a heavily disturbed signal, as already noticed by Kaluzny et al. (2013a). A similar light curve is detected at $P \simeq 0.97$ d on the previously uncatalogued ID# 8081, also an X-ray source (CX11). ID# 9050 is even more peculiar: just as ID # 275, the signal is a clean 'double-wave' at $P \simeq 0.18$ d, again an unusually short period for a cEB, but furthermore its position on the CMD is slightly *bluer* than the MS, suggesting a possible binarity with a bright WD. Only a targeted follow-up could reveal more about the nature of this target.

4 DISCUSSION AND CONCLUSIONS

In the previous sections, we described how we performed a search for photometric variability among a sample of 9410 stars in a field imaged by *HST* on the core of the GC M 4. Such a search yielded 38 variable stars; all but two are cluster members, and 20 are reported here for the first time. Quite surprisingly, two newly (re-)classified sources are a pair of bright but blended RR Lyrae, whose true nature has been unveiled by the superior angular resolution of space-based imaging. A few candidates cannot be assigned to standard variability classes, being aperiodic, multiperiodic, or lying in unusual regions of the CMD.

We did not detect any signal which could be interpreted as a transit by planet-sized objects orbiting around solar-type stars (i.e. box-shaped eclipses having photometric depth smaller than 0.03 mag). Many intrinsic factors in our data set are strongly limiting a transit search, above all sparse temporal sampling (which decreases phase coverage, and worsens the effects of long-term stellar variability) and large-scale dithering (which boosts position-dependent systematic errors). As only planets among the relatively rare 'hot Jupiter' class are within reach of such a search, the statistical significance of our null detection is probably very low. We will investigate this further in a forthcoming paper of the 'M 4 core project' series focused on transit search, which will also analyse time series photometry from the parallel ACS fields.

The overall completeness level of our search is difficult to quantify without posing very special assumptions about the shape and period of the photometric signal to be recovered. However, we note that we firmly detected variables having photometric amplitudes of the order of a few hundredths of magnitude even in the fainter half of our sample (such as ID# 1001, 3487, 3575, 5286). Even though periodograms are aliased at some characteristic frequencies by the particular sampling cadence of our data (Fig. 2), phase coverage is complete up to periods of about six days. Merging the picture, this means that eclipsing contact binaries should be detectable with a completeness factor close to 1, with only rare exceptions expected from very grazing systems, or from binaries with mass ratios *q* much smaller than 1.

About half of the reported variables (21, of which 19 are high-confidence cluster members) are certain or probable eclipsing binaries. As we detected 19 EBs among 5488 MS stars with
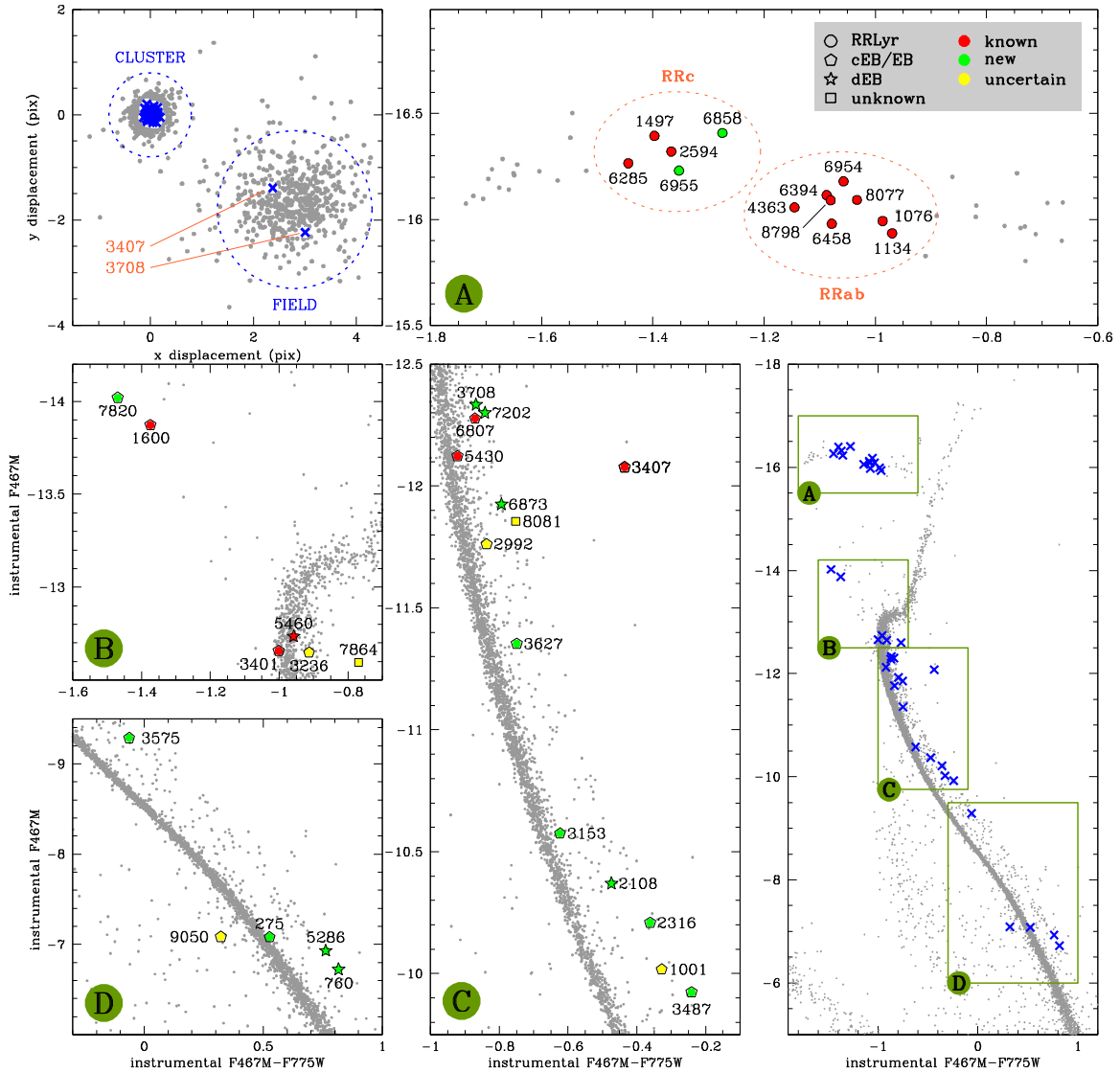
Figure 3. Proper motion vector–point and colour–magnitude diagrams (VPD, CMDs) of M 4, where the detected variables have been highlighted. Upper left: *x* and *y* proper motion displacements in physical pixels, for each analysed star (grey dots) and detected variables (blue crosses). Among the latter, only ID#3407 and 3708 appear to not be cluster members. Lower right: instrumental *F467M*, *F775W* CMD of M 4 from our data set. Variables are marked with blue crosses. Regions within green boxes (A, B, C, D) are zoomed and displayed in the corresponding remaining panels, and labelled according to the legend.

$-12.75 < F467M < -7.0$, or – restricting the magnitude range to brighter targets – 16 EBs among 4080 MS stars with $-12.75 < F467M < -9.0$, we estimate an *observed* EBs fraction of about 0.3–0.4 per cent. This value is approximately consistent with the measured photometric binary fraction in the core of 14.8 ± 1.4 per cent (Milone et al. 2012), when allowance is made for the low fraction of binaries which are expected to exhibit eclipses. Using population synthesis, Söderhjelm & Dischler (2005) show that the fraction of all F and G stars exhibiting eclipses with a depth of a few tenths of a magnitude and a period of a day is about 3 per cent. The population they studied had a binary fraction of 80 per cent, however, and so the corresponding result for the core of M 4 would be expected to be about 0.5 per cent, i.e. close to our results. A more precise discussion depends on several factors, such as the details of the period distribution of the observed binaries, dynamical erosion of the binary population, and the initial binary distributions assumed

in the population synthesis. Indeed, the observations reported in this paper are likely to be a useful constraint on our future dynamical modelling of M 4.

As a final remark, we note that the dEBs that are cluster members can potentially be used for obtaining precise cluster parameters, insights into multiple populations of the cluster and stellar evolution tests in general (Paper I; Brogaard et al. 2012; Milone et al. 2014). This requires however that the dEBs are bright enough for spectroscopic measurements. Based on our experience from dEBs in the open cluster NGC 6791, four of the dEBs we identify in M 4 (ID# 5460, 7202, 6873, and 2108) are within reach of current spectroscopic facilities such as Ultraviolet and Visual Echelle Spectrograph at the Very Large Telescope. Adding also the additional dEBs found and analysed by Kaluzny et al. (2013b) makes a sample of six dEBs in the turn-off and upper MS of M 4 with great potential for improved cluster insights. The two low-mass dEB systems
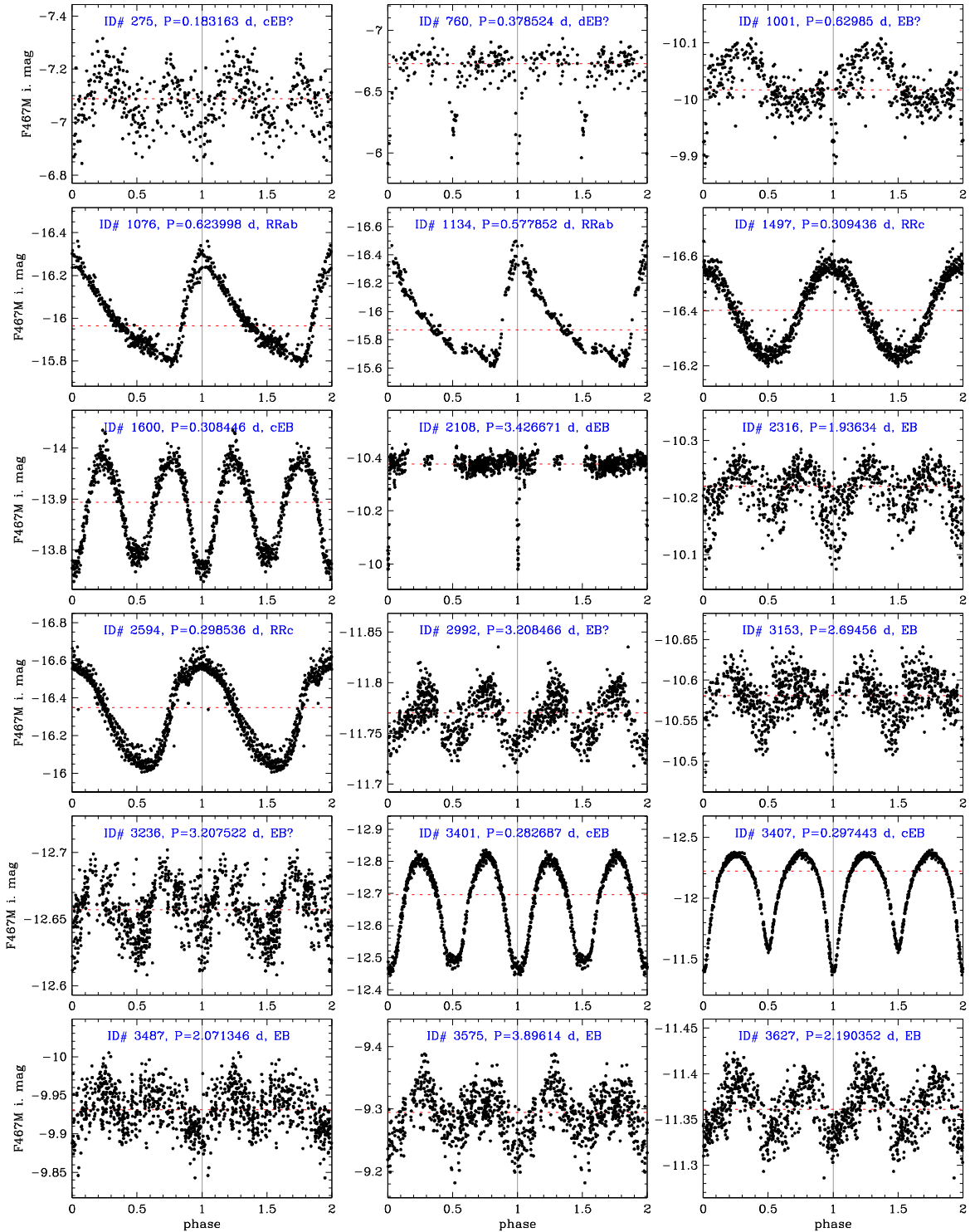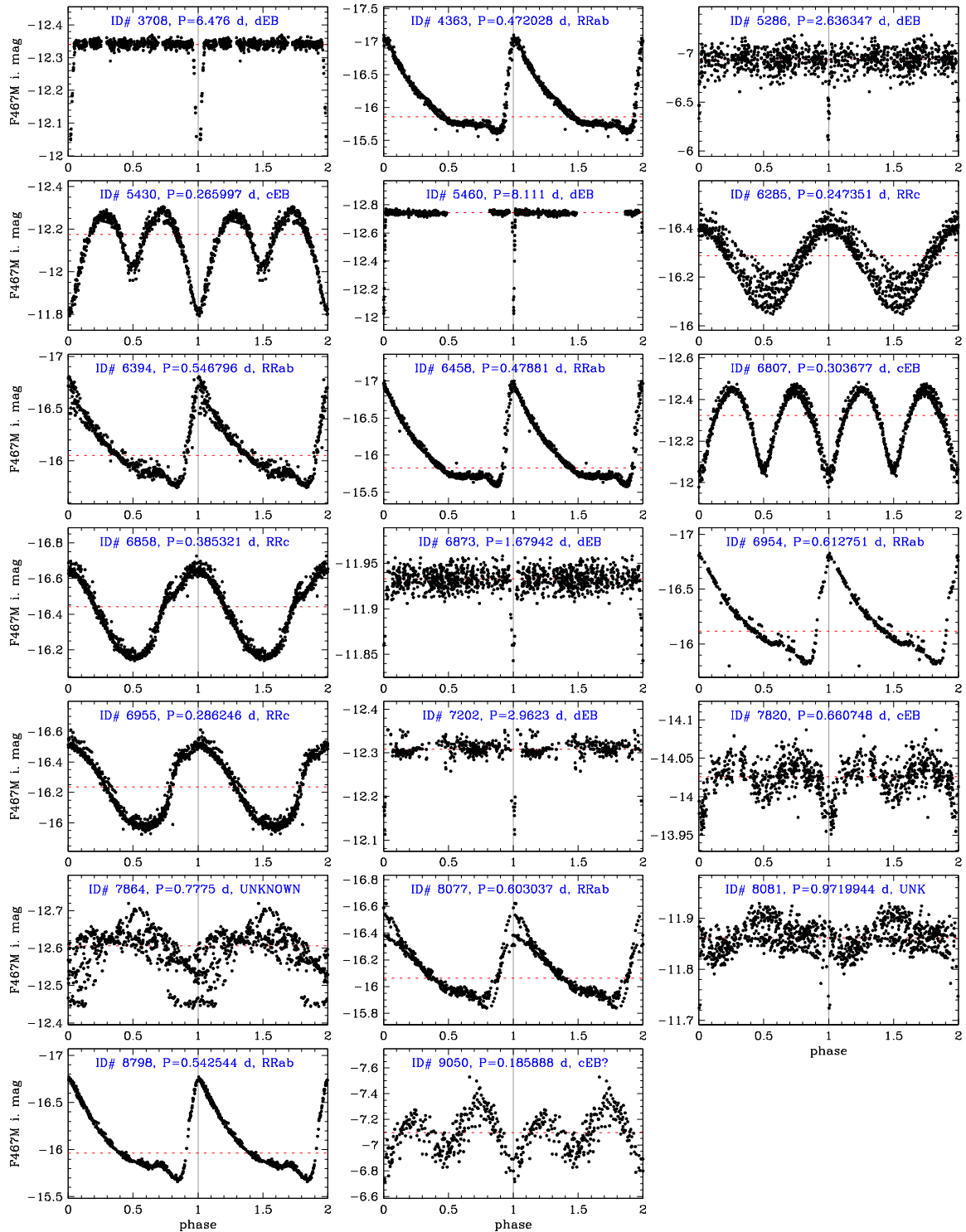
Figure 4. Light curves of variables detected on our data set, folded on the most significant period found by periodograms (ID# 275–3627). Data points are repeated twice over phase for clarity. Targets are sorted by ID# code. See Table 1 for coordinates and cross-referencing.

found on the lower MS ($V \simeq 22$; ID# 760 and 5286) are too faint for current spectroscopic facilities, but interesting potential targets for a future extremely large telescope. We note that M 4 will be in one of the fields of the K2 mission (Howell et al. 2014), and that observing these six dEBs with K2 would solve period ambiguities and provide full-coverage light curves valuable for their analysis.

ACKNOWLEDGEMENTS

Figure 5. Light curves of variables detected on our data set, folded on the most significant period found by periodograms (ID# 3708–9050). Data points are repeated twice over phase for clarity. Targets are sorted by ID# code. See Table 1 for coordinates and cross-referencing.

ASTROMETRY.NET codes (Lang et al. 2010). This research made use of the International Variable Star Index (VSX) data base, operated at AAVSO, Cambridge, MA, USA.

REFERENCES

Anderson J., King I. R., 2000, PASP, 112, 1360

Anderson J. et al., 2008, AJ, 135, 2055

Bassa C. et al., 2004, ApJ, 609, 755

Bedin L. R., Salaris M., Piotto G., Anderson J., King I. R., Cassisi S., 2009, ApJ, 697, 965

Bedin L. R. et al., 2013, Astron. Nachr., 334, 1062

Brogaard K. et al., 2012, A&A, 543, A106

Clement C. M. et al., 2001, AJ, 122, 2587

de Sitter A., 1947, Bull. Astron. Inst. Neth., 10, 287

Eastman J., Siverd R., Gaudi B. S., 2010, PASP, 122, 935

Ferdman R. D. et al., 2004, AJ, 127, 380

Gilliland R. L., 2004, Instrument Science Report ACS 2004-01: ACS CCD Gains, Full Well Depths, and Linearity up to and Beyond Saturation. STScI, Baltimore

Gilliland R. L., Rajan A., Deustua S., 2010, Instrument Science Report WFC3 2010-10: WFC3 UVIS Full Well Depths, and Linearity Near and Beyond Saturation. STScI, Baltimore

Greenstein J. L., 1939, ApJ, 90, 387

Harris W. E., 1996, AJ, 112, 1487

Hartman J. D., Gaudi B. S., Holman M. J., McLeod B. A., Stanek K. Z., Barranco J. A., Pinsonneault M. H., Kalirai J. S., 2008, ApJ, 675, 1254

Heggie D., Hut P., 2003, The Gravitational Million-Body Problem: A Multi-disciplinary Approach to Star Cluster Dynamics. Cambridge Univ. Press, Cambridge

Howell S. B. et al., 2014, PASP, 126, 398

Kaluzny J., Thompson I. B., Krzeminski W., 1997, AJ, 113, 2219

Kaluzny J., Rozanska A., Rozyczka M., Krzeminski W., Thompson I. B., 2012, ApJ, 750, L3

Kaluzny J., Thompson I. B., Rozyczka M., Krzeminski W., 2013a, Acta Astron., 63, 181

Kaluzny J. et al., 2013b, AJ, 145, 43

Kovács G., 2009, in Guzik J. A., Bradley P. A., eds, AIP Conf. Proc., Vol. 1170, Stellar Pulsation: Challenges for Theory and Observation. Am. Inst. Phys., New York, p. 261

Kovács G., Zucker S., Mazeh T., 2002, A&A, 391, 369

Lang D. et al., 2010, AJ, 139, 1732

Leavitt H. S., Pickering E. C., 1904, Harv. Coll. Obs. Circ., 90, 1

Lomb N. R., 1976, Ap&SS, 39, 447

Milone A. P. et al., 2012, A&A, 540, A16

Milone A. P. et al., 2014, MNRAS, 439, 1588

Nascimbeni V., Bedin L. R., Piotto G., De Marchi F., Rich R. M., 2012, A&A, 541, A144

Nefs S. V. et al., 2012, MNRAS, 425, 950

Norton A. J. et al., 2011, A&A, 528, A90

Pont F., Zucker S., Queloz D., 2006, MNRAS, 373, 231

Sarajedini A. et al., 2007, AJ, 133, 1658

Sawyer H. B., 1931, Harv. Coll. Obs. Circ., 366, 1

Scargle J. D., 1982, ApJ, 263, 835

Schwarzenberg-Czerny A., 1989, MNRAS, 241, 153

Shokin Y. A., Samus N. N., 1996, Astron. Lett., 22, 761

Sigurdsson S., Richer H. B., Hansen B. M., Stairs I. H., Thorsett S. E., 2003, Science, 301, 193

Söderhjelm S., Dischler J., 2005, A&A, 442, 1003

Tamuz O., Mazeh T., Zucker S., 2005, MNRAS, 356, 1466

Trager S. C., King I. R., Djorgovski S., 1995, AJ, 109, 218

Zechmeister M., Kürster M., 2009, A&A, 496, 577

SUPPORTING INFORMATION

Additional Supporting Information may be found in the online version of this article:

Table 2. Light curves of the variables found (http://mnras.oxfordjournals.org/lookup/suppl/doi:10.1093/mnras/stu930/-/DC1).

Please note: Oxford University Press is not responsible for the content or functionality of any supporting materials supplied by the authors. Any queries (other than missing material) should be directed to the corresponding author for the paper.

This paper has been typeset from a TEX/LATEX file prepared by the author.